Comparative Medicine
Copyright 2019
by the American Association for Laboratory Animal Science

Vol 69, No 1
February 2019
Pages 22–28

Original Research

Development of an Orthotopic Intrasplenic Xenograft Mouse Model of Canine Histiocytic Sarcoma and Its Use in Evaluating the Efficacy of Treatment with Dasatinib

Marilia Takada,[1,†] Lauren A Smyth,[1] Jeremy ML Hix,[2] Sarah M Corner,[4] Sandra O'Reilly,[3] Matti Kiupel,[4] and Vilma Yuzbasiyan-Gurkan[1,*]

Canine histiocytic sarcoma is a highly aggressive and metastatic hematopoietic neoplasm that responds poorly to currently available treatment regimens. Our goal was to establish a clinically relevant xenograft mouse model to assess the preclinical efficacy of novel cancer treatment protocols for histiocytic sarcoma. We developed an intrasplenic xenograft mouse model characterized by consistent tumor growth and development of metastasis to the liver and other abdominal organs. This model represents the metastatic or disseminated form of canine histiocytic sarcoma, which is considered the most clinically challenging form of the disease. Transfection of tumor cells with a luciferase vector supported the use of in vivo bioluminescence imaging to track tumor progression over time and to assess the response of this murine model to novel chemotherapeutic agents. Dasatinib treatment of the mice with intrasplenic xenografts decreased tumor growth and increased survival times, compared with mice treated with vehicle only. Our findings indicate the potential of dasatinib for the treatment of histiocytic sarcoma in dogs and for similar diseases in humans. These results warrant additional studies to clinically test the efficacy of dasatinib in dogs with histiocytic sarcoma.

Abbreviations: BLI, noninvasive bioluminescence imaging; HS, histiocytic sarcoma; IVIS, in vivo imaging system

DOI: 10.30802/AALAS-CM-18-000065

Canine histiocytic sarcoma (HS), historically called malignant histiocytosis, is a highly aggressive hematopoietic neoplasm of malignant cells of dendritic cell lineage. Although rare (fewer than 1% of all cancers),[5] several dog breeds are highly predisposed to HS, including Bernese mountain dogs (more than 25% of the population),[1,10] flat-coated retrievers,[11,12] golden retrievers, and Rottweilers.[2,7,30] Canine HS most frequently develops in the spleen, lymph nodes, liver, lung, and bone marrow,[2,23] where it progresses rapidly, disseminating to multiple organs in 70% to 91% of cases.[7,12,23,30] Due to the lack of effective options for treatment, patients respond poorly to available protocols, resulting in survival times that range from a few weeks to 3 mo.[14,28,30]

Studies by our group using HS cell lines in culture have indicated dasatinib as a potential treatment option for dogs with HS.[34] Other research groups shared similar results after testing dasatinib in HS cell lines[17] and in a subcutaneous xenograft mouse model of HS.[18] Dasatinib is a tyrosine kinase inhibitor of multiple targets including SRC family kinases (SRC, LCK, YES, and FYN). This drug is approved for people with Philadelphia chromosome–positive chronic myeloid leukemia or acute lymphoblastic leukemia.[31] The efficacy of dasatinib in dogs and humans with HS is unknown.

Human HS is a similar and equally aggressive malignancy to canine HS and is extremely rare, accounting for less than 1% of all hematopoietic neoplasms.[19,20] In humans, HS is associated with a poor prognosis and a survival time of less than 1 y.[24,38] Human HS may present as a localized disease that is treatable with surgical resection or radiation therapy; however, it typically presents at an advanced stage that involves multiple organs, including lymph nodes, the gastrointestinal tract, spleen, and lungs.[16,29,35] Patients with disseminated disease have a poor prognosis due to limited response to available treatments.[13,16] Studies to identify more effective therapeutic approaches are warranted, but given the low incidence of HS in humans, research progress is slow. Dogs are the only species that spontaneously develops a similar form of HS at an appreciable frequency, thus representing an important translational model for this rare disease in humans.

Xenograft mouse models are important tools to evaluate the in vivo response to novel cancer therapeutic interventions. Although no human HS xenograft model has been reported in the literature to date, xenograft models of subcutaneous canine HS were successfully established in 2 studies, but neither of these models developed metastatic disease.[3,39] Other authors described a xenograft model that presented as disseminated

Received: 01 Jun 2018. Revision requested: 29 Jun 2018. Accepted: 22 Aug 2018.
[1]Comparative Medicine and Integrative Biology Program, [2]Department of Radiology, [3]Research Technology Support Facility, and [4]Pathobiology and Diagnostic Investigation, College of Veterinary Medicine, Michigan State University, East Lansing, Michigan
[*]Corresponding author. Email: vygsu@msu.edu
[†]Current affiliation: Department of Surgical Sciences, School of Veterinary Medicine, University of Wisconsin, Madison, Wisconsin

disease when canine HS cells were injected intravenously into SCID mice.[37] Although this model mimicked metastatic behavior, the study included only 3 mice, and an effective method for tracking tumor progression over the course of the study was not described, thus limiting the model's applicability.

The goal of our current study was to establish a clinically relevant animal model of HS by transplanting cells derived from an HS neoplasm in a Bernese mountain dog into immunodeficient mice and to test the utility of the resulting mouse model in evaluating the treatment efficacy of novel drugs. We first report an interesting phenomenon of spontaneous regression of subcutaneous xenograft tumors in mice, which was associated with necrosis and an inflammatory process enriched with a neutrophilic population. However, after injecting the HS cells into a more orthotopic site, the spleen, we observed consistent tumor growth and development of metastasis to the liver and neighboring organs. Using HS cells transfected with a luciferase vector allowed us to perform studies in fewer mice per group and to follow in detail the growth and distribution of tumors in this model. In addition, the intrasplenic xenograft model was suitable to assess response to therapy, showing a promising response to dasatinib, a multikinase inhibitor, previously reported by our group and others as a potential approach for treating canine HS.[17,18,34]

Our orthotopic intrasplenic xenograft model recapitulates an aggressive, metastatic form of HS and is a useful tool for predicting the efficacy of cancer agents. This model provides valuable preclinical information regarding novel treatment approaches for canine HS that can translate to similar diseases in humans.

Materials and Methods

Cell culture establishment. The BD cell line originated from an HS neoplasm of a Bernese mountain dog. A comprehensive characterization of this cell line was recently reported by our group.[34] Briefly, to isolate tumor cells for cell culture, a sample of tumor tissue was minced by using a surgical blade and placed in 1% collagenase (catalog no. C9891, Sigma, St Louis, MO) in complete medium for disaggregation. After incubation for at least 1 h, the collagenase-containing solution was thoroughly washed away by using PBS, and tumor-derived cells were plated in RPMI 1640 (catalog no. 11875-093, ThermoFisher, Waltham, MA) supplemented with 10% heat-inactivated fetal bovine serum (catalog no. 10100147, ThermoFisher), 1% 100× antibiotic–antimycotic solution (catalog no. 10378016, ThermoFisher), and 0.1% gentamycin (catalog no. 15710064, ThermoFisher) and incubated at 37 °C in 5% CO_2.

Transfection of cancer cells with a luciferase expression vector. BD cells from cryopreserved vials from early passages were transfected with a luciferase expression vector to enable cell tracking by noninvasive bioluminescence imaging (BLI). Briefly, cells were incubated with vector pGL4.51 (*luc2*/CMV/Neo; catalog no. E1320, Promega, Madison, WI) and Lipofectamine 2000 reagent (catalog no. 11668027, ThermoFisher) for a maximum of 48 h. Transfected cells were selected by using G418 (140 µg/mL; Geneticin, ThermoFisher) for 10 d. Transfection efficacy was evaluated in vitro, where bioluminescence signal was detected in a population of as few as 12,500 cells. BD cells stably transfected with the luciferase vector are hereafter referred to as 'BD-luc cells'.

Harvesting HS cells from culture for injection into mice. To maximize their viability, cultured HS cells were given fresh complete media on the day before surgery and, for injection, were harvested during exponential growth (that is, approximately 70% to 80% confluency). BD-luc cells in complete media were mixed 1:1 with Matrigel (catalog no. CB-40234C, Corning, Corning, NY) to final concentrations of 1×10^8 cells/mL (1×10^7 cells per 100 µL) and 2×10^7 cells/mL (1×10^6 cells per 50 µL) for subcutaneous and intrasplenic injection, respectively, and kept on ice until use. HS cells were prepared for injection as close as possible to the time of injection.

Subcutaneous xenograft mouse model. At 1 d prior to surgery, hair was removed from the right rear flanks of anesthetized female NOD scid γ mice (n = 5; age, 7 wk; NOD.Cg-Prkdc^{scid} Il2rg^{tm1Wjl}/SzJ, The Jackson Laboratory, Bar Harbor, ME) by using depilatory cream (Nair, Church and Dwight, Ewing, NJ). A total of 100 µL of cell suspension containing 10×10^6 BD-luc cells was inoculated subcutaneously into the right rear flank of each anesthetized mouse by using a syringe with a 25-gauge needle. Weekly noninvasive BLI and biweekly caliper measurements were performed to monitor tumor growth. All animal studies were performed in accordance with institutional guidelines and were approved by the IACUC at Michigan State University.

Intrasplenic orthotopic xenograft mouse model. For the intrasplenic xenograft model, hair was removed from the left thoracic and abdominal area of immunodeficient female NOD scid γ anesthetized mice (n = 10; age, 6 wk; NOD.Cg-*Prkdc^{scid} Il2rg^{tm1Wjl}*/SzJ, The Jackson Laboratory) by using depilatory cream (Nair, Church and Dwight). The following day, mice were anesthetized, and BD-luc cells were injected into the spleen through a laparotomy approach.

Description of the surgical procedure for intrasplenic injection. A class II type A2 biologic safety cabinet was used for all procedures. Sterile drapes were placed over the working areas to help maintain a clean environment **(**Figure 1 A**)**. Mice were anesthetized by using isoflurane. Initially animals were placed inside a small anesthesia induction chamber in which the percentage of isoflurane was as high as 4% in 0.8 L/min oxygen; for maintenance, mice were placed in right lateral recumbency over a heating pad at the nose cone of a nonrebreathing circuit providing 1.5% to 2.0% isoflurane **(**Figure 1 C**)**. Eye ointment was applied to avoid dryness, and a rectal probe was placed to monitor body temperature during surgery.

The surgical site was aseptically prepared by using 3 rounds of alternating sterile solutions (saline, 4% chlorhexidine gluconate, and 10% povidone–iodine solution) and covered with a sterile paper drape. The skin was incised (approximately 1 cm) at the level of the spleen by using a no. 15 scalpel blade and by lifting the skin with forceps to avoid damaging underneath structures (Figure 1 D). At this point, the spleen appeared through the translucent abdominal wall as a dark-colored linear structure.

The abdominal wall was incised by using scissors at the level of the spleen, which was partially exteriorized by gently pulling on the underlying fat (Figure 1 E and F). When necessary, a cotton-tipped swab was used to push the stomach cranially to better expose the spleen. Warm sterile saline solution was applied to keep the spleen moist.

The tumor cell suspension, which was kept on ice, was gently homogenized, and a total volume of 50 µL containing 1×10^6 BD-luc cells was mixed 1:1 with Matrigel (Corning) was loaded into a 30-gauge insulin syringe (catalog no. 328411, Becton Dickinson). he syringe needle was inserted into the lower pole of the spleen cranially (about 0.3 to 0.4 mm; Figure 1 G), and the contents were slowly discharged as the needle was pulled out caudally. Once the cell injection was complete, the needle was slowly removed, and a small amount of absorbable hemostasis material (catalog no. 1961, Surgicel Fibrillar, Ethicon, Somerville, NJ) was placed over the injection site and pressed with a

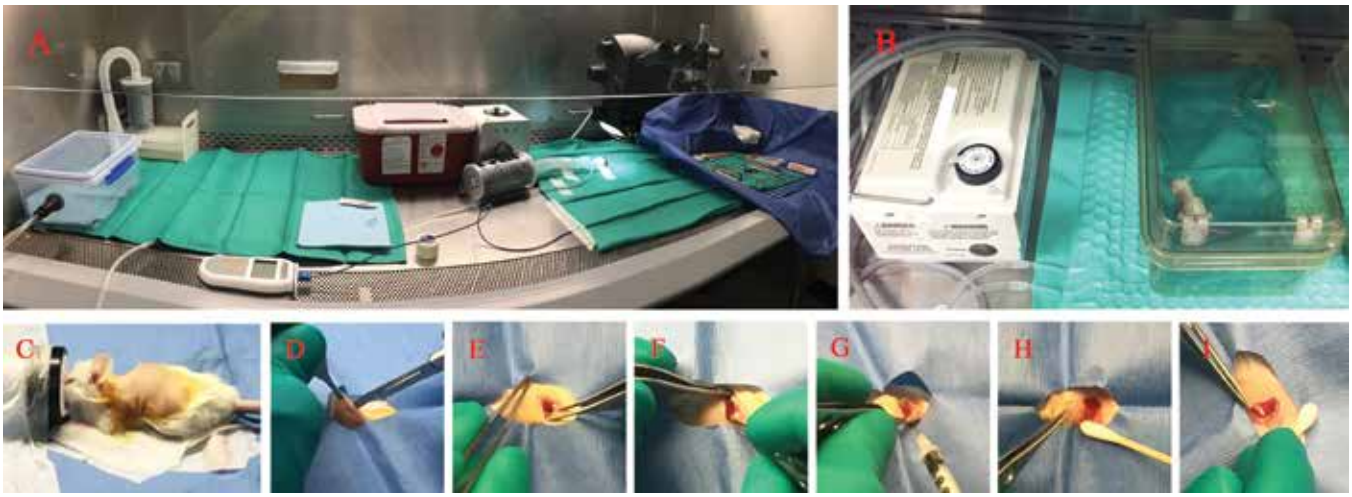

Figure 1. Surgical procedure for intrasplenic injection of cells through a laparotomy approach. (A and B) An aseptic field is prepared for surgical procedures and postoperative monitoring. The mouse is positioned in right lateral recumbency under gas anesthesia (2% to 4% isoflurane). (D through F) The spleen is accessed through a skin incision made by using a surgical blade, followed by access into the abdominal musculature by using surgical scissors. (G) A total of 1×10^6 BD-luc cells is injected into the spleen by using a 30-gauge insulin syringe, and (H) absorbable hemostasis material is placed over the site of injection. (I) The spleen expands and appears light in color after delivery of the cell suspension.

cotton-tipped swab to ensure adequate hemostasis (Figure 1 H and I).

The spleen was gently pushed back into the abdominal cavity, and the incision closed in 2 layers (abdominal wall and skin) by using 5-0 absorbable suture (catalog no. PDP303, PDS II Plus, Ethicon) in a simple interrupted pattern. To prevent loss of fluids, 300 µL of warm saline solution was given subcutaneously in the dorsal region. Mice were placed inside sterile cages over water blankets for recovery, until they were mobile and breathing regularly (Figure 1 B).

For analgesia, preoperative medication consisting of buprenorphine (0.05 mg/kg SC) and meloxicam (1 mg/kg SC) was administered about 20 min prior to surgery. Postoperative analgesia included buprenorphine (0.05 mg/kg SC twice daily) and meloxicam (1 mg/kg SC daily) y for 48 h. Mice were monitored daily and their behavior and health assessed, as described in the next section.

Treatment protocol and health assessment. At 15 d after cell injection, mice were randomly divided into 2 treatment groups of 5 mice each. Mice were treated daily with either dasatinib (30 mg/kg IP; catalog no. 11498, Cayman) or vehicle (10% β-cyclodextrin, catalog no. 16169, Cayman). The dasatinib treatment protocol was based on a previous study,[9] where 30 mg/kg IP was well tolerated with minimal side effects in mice. Because the HS neoplasms grew internally, tumor progression was monitored by using noninvasive BLI biweekly, and health was assessed as changes in hair coat, eyes, and posture to indicate internal changes in the animal. Campus Animal Resources veterinary and animal care staff monitored the health of each mouse daily. Mice were euthanized as soon as they reached any of the following humane endpoints: abnormal bodily function (that is, difficulty in ambulation, eating, drinking, defecation, or urination); labored breathing; decreased or abnormal movement; hypothermia (cool to the touch); self-mutilation; weight loss greater than 15%; abnormal posture; and abnormal hair coat. Animals were euthanized when humane end points were reached or at 65 d after the injection of tumor cells.

In vivo BLI. Noninvasive BLI (IVIS Spectrum, Perkin Elmer, Hopkinton, MA) was used to monitor tumor growth and metastasis. Mice were injected with D-luciferin (150 mg/kg IP; LUCK-100, GoldBio, St Louis, MO) and anesthetized (2% to 2.5% isoflurane). Images were acquired at 15 min after administration of D -luciferin. Bioluminescent radiance (photons/s/cm^2/sr) from the region of interest of each animal was analyzed by using Living Image software (Perkin Elmer).

Histopathology of mouse tissues. Tissues from mice were fixed in 10% formalin for 24 h and transferred to 70% ethanol until embedded in paraffin. For each mouse, a single representative section of an organ of interest was stained with hematoxylin and eosin. For immunohistochemistry, sections from the paraffinated blocks were deparaffinized in xylene and rehydrated in ethanol at various concentrations; 3% hydrogen peroxide was used to neutralize endogenous peroxidase. Antigen retrieval of formalin-fixed, paraffin-embedded tissues was performed by using PT Link (Dako, Agilent, Santa Clara, CA) and EnVision FLEX Target Retrieval Solution (low pH; Dako) for 20 min. Sections were labeled with a monoclonal antibody against CD204 (KT022, clone SRA-E5, TransGenic, Kobe, Japan) by using an Autostainer Link 48 and the EnVision Flex+ detection system (Dako). Immunoreaction was visualized by using 3,3'diaminobenzidine substrate (Dako), and sections were counterstained with hematoxylin. Images were acquired as brightfield images under a 10× dry objective (model H600L microscope, Nikon, Tokyo, Japan). The images were displayed and analyzed by using NIS Elements AR 3.1 software (Nikon). Histopathology was assessed by a board-certified veterinary pathologist (SC).

Results

Subcutaneous xenograft HS neoplasms. On day 15 after subcutaneous injection of HS cells, there was evidence of tumor growth, according to initial increases in the BLI signal and tumor volume (Figure 2 A). All 5 mice developed a palpable subcutaneous tumor in the right flank, which reached a volume of 100 mm^3 volume at 27 and 30 d after injection. However, after a peak in growth, the BLI signal suddenly declined and tumor volume decreased (Figure 2 B). This phenomenon was associated with the skin overlying or adjacent to the tumors becoming progressively dark brown to red, followed by ulceration and formation of a firm, serocellular crust (Figure 2 C).

By day 42 after injection, the BLI signal was minimal, and tumors had shrunk dramatically. Histologically, all tumors

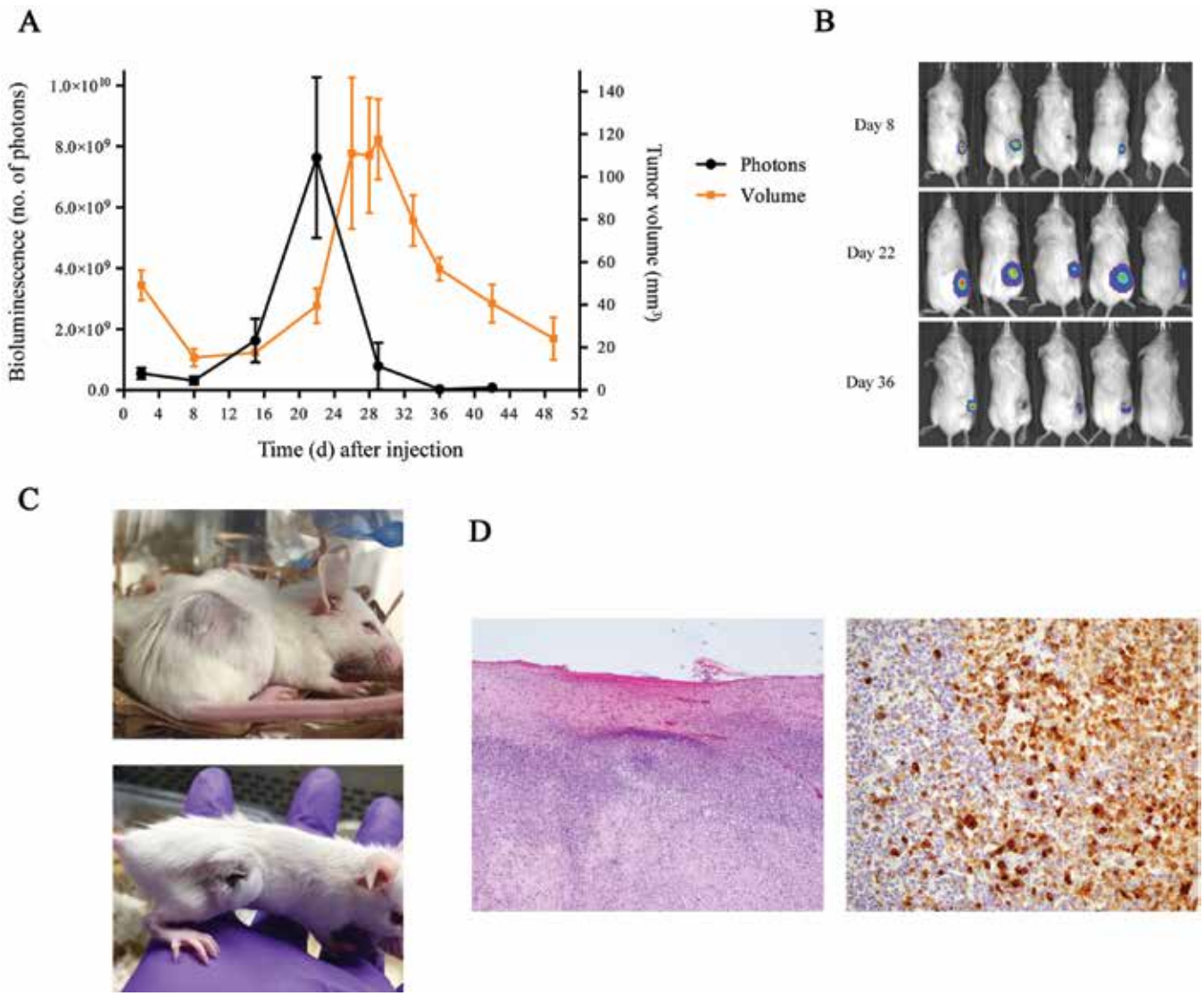

Figure 2. Subcutaneous xenograft tumors in mice showed spontaneous regression beginning 29 d after injection. (A) Increasing tumor growth based on average bioluminescent signal (black line) and total volume (orange line) was observed until days 22 and 29 after injection, respectively. Thereafter, spontaneous regression—represented as a rapid decline in these 2 parameters—occurred over time. Error bars, SEM. (B) Representations of the decrease in bioluminescence signal observed at day 36 after a peak of signal on day 22. (C) Images on day 30 showing the initial development of firm scar tissue (left) and an ulceration (black scar) covering most of the tumor (right). (D) Histiocytic sarcoma within the superficial dermis and subcutis. The overlying epidermis is ulcerated, and the surrounding superficial dermis is necrotic (left panel, hematoxylin and eosin stain). Neoplastic cells within the subcutaneous tumors show strong positive cytoplasmic immunoreactivity for CD204 (right panel). Tissue adjacent to tumor cells was negative for neutrophilic inflammation.

demonstrated necrosis and neutrophilic inflammation, albeit to different degrees. Skin lesions developed secondary to tumor growth within the superficial dermis, leading to neutrophilic inflammation and ulceration of the overlying epidermis (Figure 2 D). None of the mice presented any clinical signs related to tumor formation or regression.

Tumor growth and metastasis in the intrasplenic xenograft HS model. All 10 of the mice injected intrasplenically yielded a detectable BLI signal from day 3 after injection onward. BLI signals were detected mainly in the hypogastric region of the mice, where the spleen is located. The signal increased consistently over time for at least 27 d after injection, and mice were euthanized as the predetermined humane endpoints were reached.

At necropsy, the majority of the splenic parenchyma was replaced by a firm, tan to white mass (diameter, 1 to 1.5 cm). The liver was enlarged with rounded edges and contained numerous pinpoint tan foci on the capsular and cut surfaces, suggestive of metastatic disease (Figure 3 A). In accordance with the macroscopic findings, postmortem BLI analysis of mice showed signals in the liver and lungs (Figure 3 A). Histologically, HS metastases were present in the spleen and liver and were characterized by diffuse infiltrates of highly pleomorphic neoplastic histiocytic cells, with marked anisocytosis, anisokaryosis, and numerous multinucleated cells (Figure 3 B).

Dasatinib treatment of intrasplenic xenograft HS mice. Treatment with either dasatinib or vehicle was initiated at 15 d after injection. Biweekly BLI images showed a lower rate of signal increase in mice treated with dasatinib when compared with untreated mice, and the values of each group differed significantly ($P = 0.002$, Student t test; Figure 3 C and D). The BLI signal from control, vehicle-treated mice often decreased as the endpoint neared; this effect is related to poor vascularization as tumor gets larger, thus limiting the substrate and oxygen that generate the bioluminescent signal.[22]

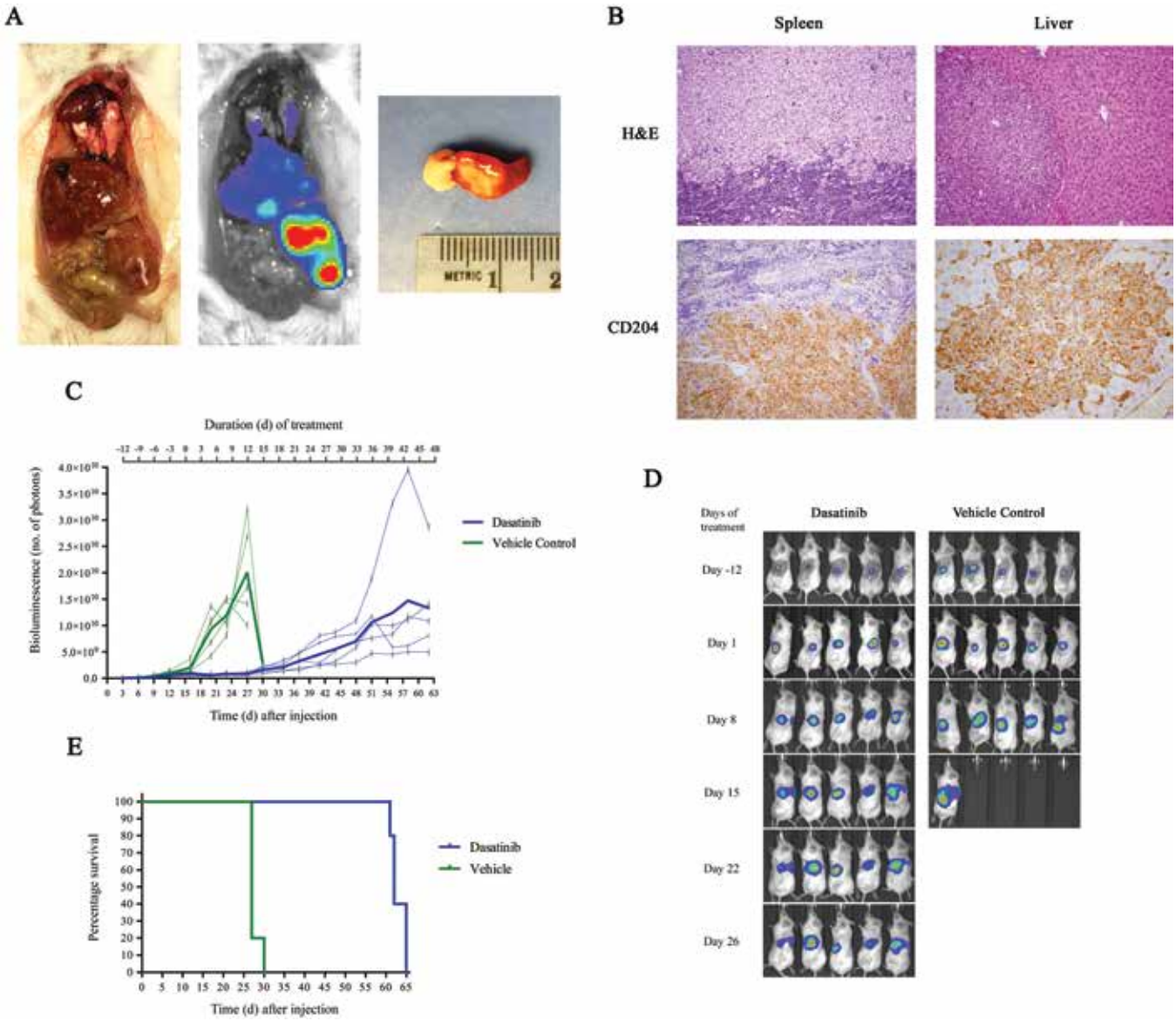

Figure 3. Intrasplenic xenograft model showed consistent tumor growth, thus enabling evaluation of the efficacy of treatment with dasatinib. (A) Intrasplenic xenograft mice developed a large tumor in the spleen, with metastasis to liver and lungs. Tumors were visible on necropsy and through ex vivo bioluminescence imaging. (B) Images of hematoxylin-and-eosin (H&E)–stained tumors in the spleen and liver, and tumor cells were positive for CD204. (C) Mice treated with dasatinib had a significantly (P = 0.002, Student t test) lower rate of tumor growth, when compared with untreated mice; (D) in the graph, the thick lines represent the mean values of each group. (E) Kaplan–Meier survival curves show that mice treated with dasatinib survived twice as long as untreated mice, and this difference in survival is statistically significant (P = 0.0016, Mantel–Cox test).

Treatment with either dasatinib or vehicle continued until mice reached predetermined endpoints, when they were euthanized. Whereas control mice reached these endpoints on day 27 (n = 4) and day 30 (n = 1) after injection, mice treated with dasatinib were euthanized due to poor health on days 61 (n = 1), 62 (n = 2), and 65 (n = 2). Kaplan–Meier survival time (Figure 3 E) was significantly (P = 0.0016, Mantel–Cox test) longer in mice treated with dasatinib than in vehicle-only control mice.

Metastatic lesions were present in all mice. However, the extent of metastatic disease could not be compared between treatment groups, because animals were euthanized at different time points throughout the study, when humane endpoints were reached and when disease was at an advanced stage.

Discussion

Xenograft mouse models are an important preclinical tool for the evaluation of novel drug treatment approaches. However, establishing a model with clinical relevance can be challenging in regard to the site of implantation and the effects of the surrounding microenvironment on tumor growth. We observed an interesting phenomenon in the subcutaneous xenograft mice, in which tumors regressed spontaneously after a peak of growth. The regressed tumors showed various degrees of necrosis and neutrophilic inflammation but no signs of infection. We hypothesize that neovascularization was insufficient to support the rapid tumor growth, leading to ischemic necrosis and triggering an innate immune system response. Similar findings were reported when breast cancer cells were injected subcutaneously in mice, resulting in necrosis; the phenomenon was prevented when cells were injected into the mammary fat pad, which is considered a more orthotopic site.[15] The injection of tumor cells into orthotopic sites has been shown to produce xenograft models more efficiently and with a higher 'take rate' than ectopic injections (72% to 90% compared with 3% to 58%).[8,15,21,26,32]

Spontaneous tumor regression is a biologic phenomenon frequently observed in canine cutaneous histiocytoma, a benign form of histiocytic disorder of Langerhans cells that forms in the superficial dermis to epidermis and that typically affects dogs younger than 3 y.[36] The regression of cutaneous histiocytoma is associated with lymphocytic infiltration and necrosis of tumor histiocytes.[6] Infiltration by cytotoxic T lymphocytes that mediate the lysis of neoplastic cells has been postulated as a mechanism of tumor regression.[27] In contrast, tumor regression in our xenograft model was associated with neutrophilic infiltration, suggesting that the mechanism in the mice may be distinct from that of canine histiocytoma, although the mechanisms of tumor regression are not yet fully understood.

Our intrasplenic xenograft mouse model represents an orthotopic model for HS, providing consistent tumor growth in all 10 of the mice in the current study and in a recently published study.[33] Additional studies in our laboratory with a larger number of mice (n = 60) injected intrasplenically with HS BD-luc cells demonstrated a high level of reproducibility for this model, with consistent 100% tumor take and growth rates (data not shown). Importantly, splenic tumors had the capability to metastasize to other organs, including the liver and lungs, thus indicating that our intrasplenic xenograft model mimics a metastatic–disseminated form of HS, which is considered to be the most clinically challenging form and refractory to available treatment options. Similarly, other authors showed that intrasplenic injection of colon cancer cells resulted in large splenic tumors and liver micrometastasis in more than 50% of cases.[4]

Dasatinib is a potent in vitro inhibitor of HS cells derived from Maltese, Shetland sheepdogs, flat-coated retrievers, and golden retrievers[17] and, more recently, of HS cells from a Bernese mountain dog.[34] We successfully recapitulated our in vitro findings regarding dasatinib by using our intrasplenic xenograft mouse model. Mice with intrasplenic xenograft HS and treated with dasatinib had significant (P = 0.002) suppression of tumor growth. More importantly, mice treated with dasatinib had a significant (2-fold, P = 0.0016) increase in survival time when compared with mice treated with vehicle only. Our results confirm previously reported findings indicating that dasatinib effectively inhibits tumor growth in subcutaneous xenograft mice models of canine HS.[18] Dasatinib is a multityrosine kinase inhibitor that targets the SRC family kinases (SRC, LCK, YES, and FYN) and has been approved for people with Philadelphia-chromosome–positive chronic myeloid leukemia or acute lymphoblastic leukemia.[31] The efficacy of dasatinib in human HS is unknown. In dogs, reports of dasatinib use are limited to 2 studies, where it was used to treat a total of 4 dogs with osteosarcoma. A dasatinib dose of 0.75 mg/kg PO was administered daily for 6.5 to 25 mo and was considered safe and well tolerated.[9,25]

In conclusion, we established an intrasplenic xenograft model of HS; our model represents a clinically relevant model of an aggressive form of HS and permits the study of novel treatment approaches. Furthermore, our findings indicate that dasatinib is a potential treatment for canine HS and similar human diseases. Additional studies, including proof-of-concept clinical trials testing the efficacy of dasatinib in canine HS are warranted. Although such clinical trials may be highly costly in dogs (a daily dose of dasatinib for adult humans is estimated to cost US$450), these studies may be justified as translational research and relevant for both dogs and humans.

Acknowledgments

We thank Dr Richard Neubig and Dr Mark Bailie for their feedback during the development and execution of this project. We thank the Berner–Garde Foundation and the Bernese Mountain Dog Club of America for their efforts to advance research on disorders affecting Bernese mountain dogs. We thank the following funding sources for this project: Michigan State University College of Veterinary Medicine Endowed Research Funds, including the Foster–Smith Oncology Fund, Michigan State University Graduate School, and the AKC Canine Health Foundation (grant no. 2171), LAS was supported in part by Boehringer Ingelheim Veterinary Scholars fellowship to Michigan State University. The contents of this publication are solely the responsibility of the authors and do not necessarily represent the views of the Foundation.

References

1. **Abadie J, Hedan B, Cadieu E, De Brito C, Devauchelle P, Bourgain C, Parker HG, Vaysse A, Margaritte-Jeannin P, Galibert F, Ostrander EA, Andre C.** 2009. Epidemiology, pathology, and genetics of histiocytic sarcoma in the Bernese mountain dog breed. J Hered **100 Suppl 1:**S19–S27. https://doi.org/10.1093/jhered/esp039.
2. **Affolter VK, Moore PF.** 2002. Localized and disseminated histiocytic sarcoma of dendritic cell origin in dogs. Vet Pathol **39:**74–83. https://doi.org/10.1354/vp.39-1-74.
3. **Azakami D, Bonkobara M, Washizu T, Iida A, Kondo M, Kato R, Niikura Y, Iwaki S, Tamahara S, Matsuki N, Ono K.** 2006. Establishment and biological characterization of canine histiocytic sarcoma cell lines. J Vet Med Sci **68:**1343–1346. https://doi.org/10.1292/jvms.68.1343.
4. **Bouvet M, Tsuji K, Yang M, Jiang P, Moossa AR, Hoffman RM.** 2006. In vivo color-coded imaging of the interaction of colon cancer cells and splenocytes in the formation of liver metastases. Cancer Res **66:**11293–11297. https://doi.org/10.1158/0008-5472.CAN-06-2662.
5. **Bruner SR.** 2006. Updates in therapeutics for veterinary dermatology. Vet Clin North Am Small Anim Pract **36:**39–58. https://doi.org/10.1016/j.cvsm.2005.09.011.
6. **Cockerell GL, Slauson DO.** 1979. Patterns of lymphoid infiltrate in the canine cutaneous histiocytoma. J Comp Pathol **89:**193–203. https://doi.org/10.1016/0021-9975(79)90058-6.
7. **Craig LE, Julian ME, Ferracone JD.** 2002. The diagnosis and prognosis of synovial tumors in dogs: 35 cases. Vet Pathol **39:**66–73. https://doi.org/10.1354/vp.39-1-66.
8. **Cunningham D, You Z.** 2015. In vitro and in vivo model systems used in prostate cancer research. J Biol Methods **2:**1–28.
9. **Davis LE, Hofmann NE, Li G, Huang ET, Loriaux MM, Bracha S, Helfand SC, Mata JE, Marley K, Mansoor A, Tyner JW, Abraham J, Seguin B, Keller C.** 2013. A case study of personalized therapy for osteosarcoma. Pediatr Blood Cancer **60:**1313–1319. https://doi.org/10.1002/pbc.24512.
10. **Dervisis NG, Kiupel M, Qin Q, Cesario L.** 2016. Clinical prognostic factors in canine histiocytic sarcoma. Vet Comp Oncol.**15:**1171–1180.
11. **Dobson J, Hoather T, McKinley TJ, Wood JL.** 2009. Mortality in a cohort of flat-coated retrievers in the UK. Vet Comp Oncol **7:**115–121. https://doi.org/10.1111/j.1476-5829.2008.00181.x.
12. **Fidel J, Schiller I, Hauser B, Jausi Y, Rohrer-Bley C, Roos M, Kaser-Hotz B.** 2006. Histiocytic sarcomas in flat-coated retrievers: a summary of 37 cases (November 1998 to March 2005). Vet Comp Oncol **4:**63–74. https://doi.org/10.1111/j.1476-5810.2006.00090.x.
13. **Gounder M, Desai V, Kuk D, Agaram N, Arcila M, Durham B, Keohan ML, Dickson MA, D'Angelo SP, Shukla N, Moskowitz C, Noy A, Maki RG, Herrera DA, Sanchez A, Krishnan A, Pourmoussa A, Qin LX, Tap WD.** 2015. Impact of surgery, radiation, and systemic therapy on the outcomes of patients with dendritic cell and histiocytic sarcomas. Eur J Cancer **51:**2413–2422. https://doi.org/10.1016/j.ejca.2015.06.109.
14. **Higuchi T, Dervisis N, Kitchell B**. 2011. Efficacy of doxorubicin for histiocytic sarcoma in dogs. Abstracts presented at the 30th Annual Veterinary Cancer Society Meeting Conference, San Diego, California 29 October–1 November 2010. Vet Comp Oncol **9:**e12–e12. https://doi.org/10.1111/j.1476-5829.2010.00252.x.
15. **Ho KS, Poon PC, Owen SC, Shoichet MS.** 2012. Blood vessel hyperpermeability and pathophysiology in human tumour xenograft models of breast cancer: a comparison of ectopic and orthotopic

tumours. BMC Cancer **12:**1–10. https://doi.org/10.1186/1471-2407-12-579.

16. **Hornick JL, Jaffe ES, Fletcher CD.** 2004. Extranodal histiocytic sarcoma: clinicopathologic analysis of 14 cases of a rare epithelioid malignancy. Am J Surg Pathol **28:**1133–1144. https://doi.org/10.1097/01.pas.0000131541.95394.23.
17. **Ito K, Kuroki S, Kobayashi M, Ono K, Washizu T, Bonkobara M.** 2013. Identification of dasatinib as an in vitro potent growth inhibitor of canine histiocytic sarcoma cells. Vet J **196:**536–540. https://doi.org/10.1016/j.tvjl.2012.12.016.
18. **Ito K, Miyamoto R, Tani H, Kurita S, Kobayashi M, Tamura K, Bonkobara M.** 2017. Effect of dasatinib in a xenograft mouse model of canine histiocytic sarcoma and in vitro expression status of its potential target EPHA2. J Vet Pharmacol Ther **41:**e45–e48. https://doi.org/10.1111/jvp.12449.
19. **Jaffe ES.** 1988. Histiocytoses of lymph nodes: biology and differential diagnosis. Semin Diagn Pathol **5:**376–390.
20. **Jaffe ES, Harris NL, Stein H, Vardiman JW. editors.** 2001. World Health Organization classification of tumors: pathology and genetics of tumours of haematopoietic and lymphoid tissues. Lyon (France): IARC Press.
21. **Kellar A, Egan C, Morris D.** 2015. Preclinical murine models for lung cancer: clinical trial applications. BioMed Res Int **2015:**1–17. https://doi.org/10.1155/2015/621324.
22. **Khalil AA, Jameson MJ, Broaddus WC, Lin PS, Dever SM, Golding SE, Rosenberg E, Valerie K, Chung TD.** 2013. The influence of hypoxia and pH on bioluminescence imaging of luciferase-transfected tumor cells and xenografts. Int J Mol Imaging **2013:**1–9. https://doi.org/10.1155/2013/287697.
23. **Klahn SL, Kitchell BE, Dervisis NG.** 2011. Evaluation and comparison of outcomes in dogs with periarticular and nonperiarticular histiocytic sarcoma. J Am Vet Med Assoc **239:**90–96. https://doi.org/10.2460/javma.239.1.90.
24. **Kommalapati A, Tella SH, Durkin M, Go RS, Goyal G.** 2018. Histiocytic sarcoma: a population-based analysis of incidence, demographic disparities, and long-term outcomes. Blood **131:**265–268. https://doi.org/10.1182/blood-2017-10-812495.
25. **Marley K, Gullaba J, Seguin B, Gelberg HB, Helfand SC.** 2015. Dasatinib modulates invasive and migratory properties of canine osteosarcoma and has therapeutic potential in affected dogs. Transl Oncol **8:**231–238. https://doi.org/10.1016/j.tranon.2015.03.006.
26. **McIntyre RE, Buczacki SJ, Arends MJ, Adams DJ.** 2015. Mouse models of colorectal cancer as preclinical models. BioEssays **37:**909–920. https://doi.org/10.1002/bies.201500032.
27. **Moore PF, Schrenzel MD, Affolter VK, Olivry T, Naydan D.** 1996. Canine cutaneous histiocytoma is an epidermotropic Langerhans cell histiocytosis that expresses CD1 and specific β2-integrin molecules. Am J Pathol **148:**1699–1708.
28. **Rassnick KM, Moore AS, Russell DS, Northrup NC, Kristal O, Bailey DB, Flory AB, Kiselow MA, Intile JL.** 2010. Phase II, open-label trial of single-agent CCNU in dogs with previously untreated histiocytic sarcoma. J Vet Intern Med **24:**1528–1531. https://doi.org/10.1111/j.1939-1676.2010.0588.x.
29. **Shimono J, Miyoshi H, Arakawa F, Sato K, Furuta T, Muto R, Yanagida E, Sasaki Y, Kurita D, Kawamoto K, Nagafuji K, Ohshima K.** 2017. Prognostic factors for histiocytic and dendritic cell neoplasms. Oncotarget **8:**98723–98732. https://doi.org/10.18632/oncotarget.21920.
30. **Skorupski KA, Clifford CA, Paoloni MC, Lara-Garcia A, Barber L, Kent MS, LeBlanc AK, Sabhlok A, Mauldin EA, Shofer FS, Couto CG, Sorenmo KU.** 2007. CCNU for the treatment of dogs with histiocytic sarcoma. J Vet Intern Med **21:**121–126. https://doi.org/10.1111/j.1939-1676.2007.tb02937.x.
31. **Steinberg M.** 2007. Dasatinib: a tyrosine kinase inhibitor for the treatment of chronic myelogenous leukemia and Philadelphia-chromosome–positive acute lymphoblastic leukemia. Clin Ther **29:**2289–2308. https://doi.org/10.1016/j.clinthera.2007.11.005.
32. **Stewart E, Shelat A, Bradley C, Chen X, Federico S, Thiagarajan S, Shirinifard A, Bahrami A, Pappo A, Qu C, Finkelstein D, Sablauer A, Dyer MA.** 2015. Development and characterization of a human orthotopic neuroblastoma xenograft. Dev Biol **407:**344–355. https://doi.org/10.1016/j.ydbio.2015.02.002.
33. **Takada M, Hix JML, Corner S, Schall PZ, Kiupel M, Yuzbasiyan-Gurkan V**. 2018. Targeting MEK in a translational model of histiocytic sarcoma. Mol Cancer Ther **17:**2439–2450. https://doi.org/10.1158/1535-7163.MCT-17-1273.
34. **Takada M, Parys M, Gregory-Bryson E, Vilar Saavedra P, Kiupel M, Yuzbasiyan-Gurkan V.** 2018. A novel canine histiocytic sarcoma cell line: initial characterization and utilization for drug screening studies. BMC Cancer **18:**1–13. https://doi.org/10.1186/s12885-018-4132-0.
35. **Takahashi E, Nakamura S.** 2013. Histiocytic sarcoma: an updated literature review based on the 2008 WHO classification. J Clin Exp Hematop **53:**1–8. https://doi.org/10.3960/jslrt.53.1.
36. **Taylor DO, Dorn CR, Luis OH.** 1969. Morphologic and biologic characteristics of the canine cutaneous histiocytoma. Cancer Res **29:**83–92.
37. **Thongtharb A, Uchida K, Chambers JK, Nakayama H.** 2017. Variations in histiocytic differentiation of cell lines from canine cerebral and articular histiocytic sarcomas. Vet Pathol **54:**395–404.
38. **Vos JA, Abbondanzo SL, Barekman CL, Andriko JW, Miettinen M, Aguilera NS.** 2005. Histiocytic sarcoma: a study of 5 cases including the histiocyte marker CD163. Mod Pathol **18:**693–704. https://doi.org/10.1038/modpathol.3800346.
39. **Yamazaki H, Takagi S, Hosoya K, Okumura M.** 2015. Survivin suppressor (YM155) enhances chemotherapeutic efficacy against canine histiocytic sarcoma in murine transplantation models. Res Vet Sci **99:**137–144. https://doi.org/10.1016/j.rvsc.2015.02.003.